Kavli Summer Program In Astrophysics 2021:

Fluid dynamics of the Sun and Stars

Project report

Angular momentum transport by gravito-inertial waves in intermediate-mass stars

---

Hachem Dhouib

Advisor: Ankit Barik

Collaborators: Laurène Jouve & Domenico G. Meduri

Virtual school (MPS Goettingen)

June 7th - July 16th, 2021

1 Introduction

Stars are the building blocks of galaxies so it is crucial to understand how they are formed and how they evolve. The physical processes at work inside a star strongly impact its lifespan, and its energy and chemical feedback to the interstellar medium. In the recent years, asteroseismology using space telescopes has helped us determine the interior rotation rates of many intermediate-mass stars, revealing that they lose a significant amount of angular momentum between birth and death. This implies that there are processes at work which efficiently transport angular momentum from the core to the surface. Current prescriptions of angular momentum transport in stellar evolution models are unable to reproduce observations of uniform rotation of radiative envelopes of main sequence intermediate mass stars (Aerts et al., 2019). Thus, additional transport mechanisms are needed to explain these observations. These stars, with mass greater than $1.4M_\odot$ and smaller than $8M_\odot$, have a convective core and a radiative envelope. Since angular momentum transport within convection zones is efficient due to turbulent fluid motions, we restrict ourselves to discussing angular momentum transport within radiative regions. The latter is a rotating stably stratified fluid medium in which gravito-inertial waves (GIWs) can propagate. Thus, here we attempt to characterize the angular momentum transported by GIWs and determine whether they can provide a viable transport mechanism.

We present in section 2 the different mechanisms that are thought to transport angular momentum in radiative zones of stars. Then, we focus in section 3 on the generation, propagation and dissipation of gravito-inertial waves. In section 4, we present the recent studies that have tried to tackle this problem. Thereafter, we present our contribution to studying angular momentum transport using 3D hydrodynamic simulations with the MHD code MagIC (Wicht, 2002; Gastine and Wicht, 2012). Finally, we conclude and present the perspectives of this project in section 6.

2 Mechanisms of angular momentum transport in stars

In the classical approach of stellar structure and evolution, radiative zones were supposed to be motionless. However, it was proven by asteroseismology that they are the seat of four main dynamical processes (Aerts et al., 2019):

- Meridional Circulation: a flow in the (r, θ) plane caused by the deformation of the isobars (due to the centrifugal acceleration, the Lorentz force and/or the tidal force). The radiative flux is no longer divergence free and need to be balanced by heat advection and hence, the advection of the angular momentum.
- Turbulence driven by instabilities: induced by differential rotation in the radiative zone and can be classified in three families:
  - Centrifugal instabilities due to violation of the Rayleigh criterion.
  - Baroclinic instabilities caused by the misalignment of the entropy gradient and gravity.
  - Vertical and horizontal shear instabilities.
- Magnetic fields: try to align the fluid angular velocity with the poloidal field lines (Ferraro's isorotation law). A fluid differential rotation thus leads to creation of magnetic tension resulting in an exchange of angular momentum. This homogenisation of angular velocity along field lines is mediated by Alfvén waves. Additionally, in

the case where fossil magnetic field lines in the radiative zone connect to adjacent convective zones, some differential rotation can be transmitted to the radiative zone along the field lines.

- Gravito-inertial waves (GIWs): generated by any disturbance in the stratified medium. These waves propagate through radiative zones and extract or deposit angular momentum where they are damped.

Here, we will focus only on the transport induced by GIWs. To evaluate the role of these waves in angular momentum transport, it is necessary to understand their generation, propagation, and dissipation in stellar interiors.

3 Gravito-inertial waves (GIWs)

For frequencies low compared to the rotational frequency, buoyancy is the main restoring force for oscillations, giving what are called internal gravity waves (IGWs). They are present in all fluids that are stably stratified with respect to convection. In the presence of rotation, IGWs become GIWs under the supplementary action of the Coriolis acceleration. In the low-frequency limit, The dispersion relation for gravito-inertial waves is (Unno et al., 1989)

$$\omega^2 \approx N^2 \frac{k_H^2}{k^2} + \frac{(2\vec{\Omega} \cdot \vec{k})^2}{k^2}, \tag{1}$$

where ω is frequency of the wave, $\vec{k}$ is the wave vector, k_H its horizontal component, $\vec{\Omega}$ is the rotation vector and N is the Brunt-Väisälä frequency which describes the stratification in density and entropy of the fluid. We note that $N^2 < 0$ corresponds to an instability (the Rayleigh-Taylor instability or thermal convection). And if $N^2 > 0$ the Brunt-Väisälä frequency corresponds to the frequency of the oscillations of a fluid element under the restoring force of buoyancy when it is slightly moved from its position of equilibrium. In Eq. (1), the mixed behaviour of waves is clearly identified, the two terms corresponding respectively to the dispersion relations of IGWs, $\omega^2_{\rm IGW} \approx \frac{N^2 k_H^2}{k^2}$, and of inertial waves (IWs), $\omega^2_{\rm IW} \approx \frac{(2\vec{\Omega}\cdot\vec{k})^2}{k^2}$.

In the absence of rotation and magnetism, pure IGWs propagate in stably stratified regions when $\omega < N$. But when the star is rapidly rotating, waves can be influenced by the Coriolis acceleration. In fact, in the case of sub-inertial waves for which $\omega < 2\Omega$, the propagation domain is restricted to the equatorial region, and in the case of super-inertial waves for which $\omega > 2\Omega$, the waves continue to propagate in the full spherical shell as in the non-rotating case because waves are less influenced by the Coriolis acceleration (Aerts et al., 2019). And if a magnetic field is also present, GIWs become magneto-gravito-inertial waves (MGIWs) under the additional action of the Lorentz force (fig. 1).

3.1 GIWs generation

GIWs can be generated by any disturbance to the stably stratified region. The most common and efficient mechanisms of generation are

- forcing by a companion (close star or planet): which causes a disturbance at the convective-radiative interface that generates the waves, which propagate away from the convection zone (Fig. 2),
- an adjacent turbulent convection zone:

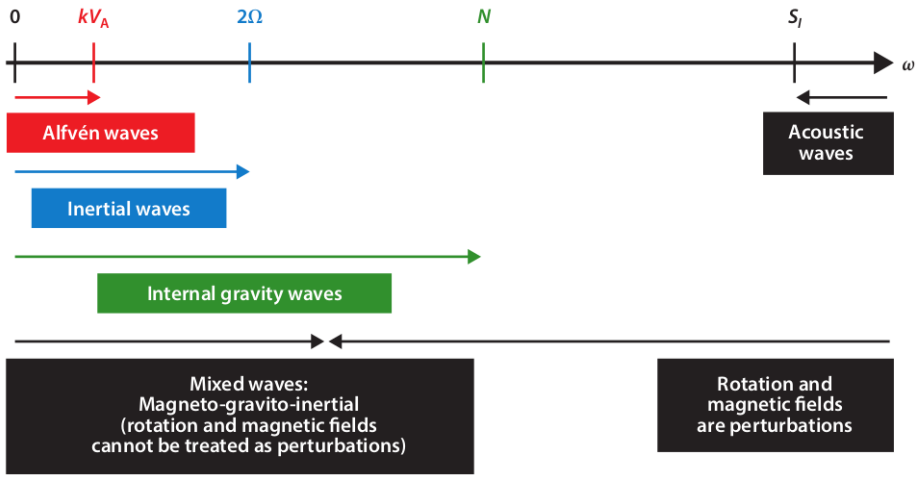

Figure 1: Types of Waves in a rotating and magnetised stably stratified radiative region.

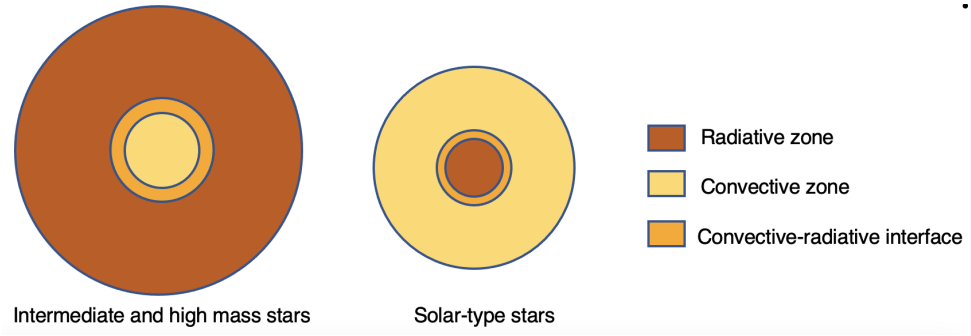

Figure 2: Configurations of the radiative and convective zones in solar-like and intermediate-mass stars.

  - bulk excitation through Reynolds stresses: caused by the convective eddies,
  - direct excitation through plumes: generated because of penetrative convection at the interface with the radiative zone. These plumes lose their kinetic energy by buoyancy and convert it into waves.

3.2 GIWs dissipation

GIWs can extract or deposit angular momentum where they are dissipated. In fact, we can distinguish three main ways of wave dissipation (Aerts et al., 2019):

- Linear thermal diffusion: arise from heat transport in the radiative interior.
- Critical layers: occur when the frequency of the wave is the same as the local rotation frequency and we get a co-rotation resonance.
- Nonlinear breaking:
  - Rayleigh-Taylor instability: overturning of the stratification (convective instability) can happen when the Brunt–Väisälä frequency approaches 0 (near convective-radiative interfaces for example).
  - Kelvin–Helmholtz instability: shear instability of the wave itself.

4 State of the art and aim of the project

4.1 State of the art

Rogers et al. (2013) preformed 2D hydrodynamic simulations of GIW generation at the boundary of the convective cores of intermediate-mass stars up to 98% of the stellar radius and studied angular momentum transport in the radiative envelope. They found signatures of wave/critical layer interactions and wave breaking that resulted in a rotational acceleration of the radiative envelope. Thereafter, Rogers (2015) used similar simulations to explain some observational constraints of the rotation profiles of intermediate and massive stars (Fig. 3a). Alvan et al. (2014, 2015) presented 3D hydrodynamic simulations of the radiative core of solar-type stars up to 97% of their radius using the ASH code (Clune et al., 1999; Brun et al., 2004, Anelastic Spherical Harmonic) to study GIWs (Fig. 3b). They calculated the spectrum of gravity modes, and showed that the spectral properties predicted by the asymptotic linear theory of stellar oscillations matched well with those obtained from the simulations. Subsequently, Augustson et al. (2016) carried out 3D MHD simulations up to 65% of stellar radius using ASH code to study the effect of rotation on the triggering of dynamo cycles in B type stars (Fig. 3c). Recently, Edelmann et al. (2019) produced the first 3D simulations of intermediate-mass stars up to 90% of the star's surface (Fig. 3d). In particular, they characterized the spectrum of wave excitation by core convection, and showed that the spectral properties of the waves were compatible with excitation by convective plumes. Furthermore, they calculated the spectrum of gravity modes present in the radiative envelope and recovered the frequencies predicted by the asymptotic linear theory of stellar oscillations, similar to Alvan et al. (2014). Finally, André (2019) preformed the first 3D hydrodynamic simulations in massive stars up to 97.5% of stellar radius (Fig. 3e) using ASH code to study angular momentum transport by GIWs. They showed that progressive waves coexist with the resonant waves (standing modes), and are responsible for more than 90% of the calculated spectral power. The contribution of these waves is highest near their excitation zone and close to the surface of the domain. They showed also that the angular momentum is deposited in the layers close to the surface of the domain, and thus a prograde rotation profile is created in this region.

Despite all these efforts that have been done, current ideas about angular momentum transport fail to explain the strong decrease of core angular momentum when stars have a convective core (Aerts et al., 2019). Thus, more detailed theoretical studies are necessary in this context.

4.2 Aim of the project

We aim to study angular momentum transport in intermediate-mass stars by GIWs using 3D hydrodynamic simulations. We achieve this by simulating an intermediate mass star as a fluid in a rotating sphere using the 3D anelastic magnetohydrodynamic (MHD) code MagIC (Wicht, 2002; Gastine and Wicht, 2012). Interior profiles of density, temperature, gravity and pressure are computed using the stellar evolution code MESA (Modules for Experiments in Stellar Astrophysics, Paxton et al., 2011, 2013, 2015, 2018, 2019). We then use these profiles in MagIC to provide us with a gravity profile and an equation of state.

5 Numerical methods

We consider a hydrodynamic simulation of a non-conducting fluid in a rotating sphere. We adopt the so-called "Lantz-Braginsky-Roberts" anelastic approximation of the Navier-

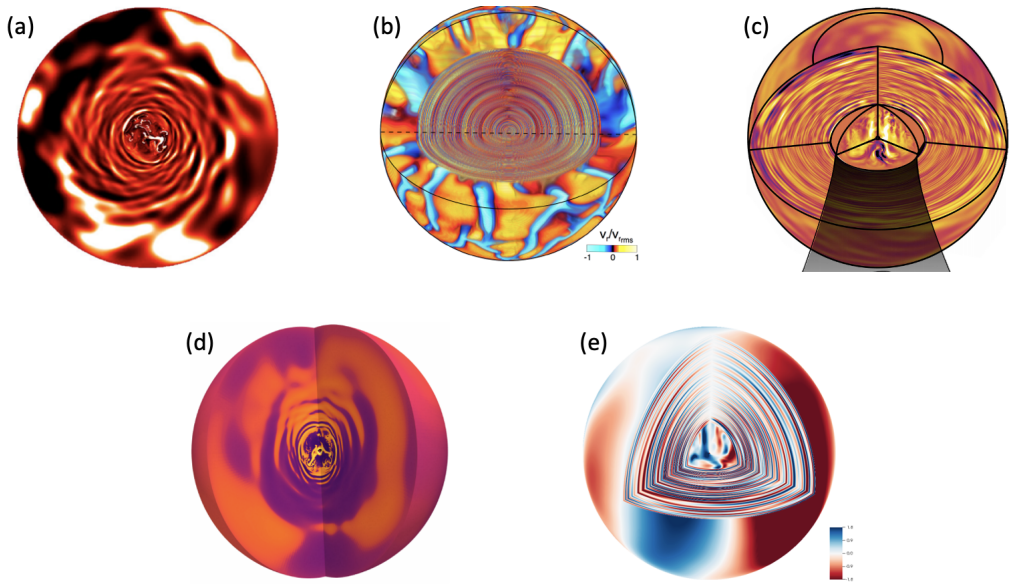

Figure 3: **(a)** Visualisation of the temperature in a 2D model of intermediate-mass star (Rogers, 2015). **(b)** 3D visualisation of the radial velocity in a solar-type star model (Alvan et al., 2014). **(c)** 3D visualisation of the radial velocity in a B type star model. **(d)** 3D visualisation of the temperature in an intermediate-mass star model (Edelmann et al., 2019). **(e)** 3D visualisation of the radial velocity in a massive star model (André, 2019).

Stokes equations (Braginsky and Roberts, 1995; Lantz and Fan, 1999). It allows the incorporation of the radial dependence of the background state while filtering out the fast acoustic waves. Within this approximation, we can solve the hydrodynamic equations for small perturbations x' around a background state $\bar{x}$ that can depart from the adiabat :

$$x(r,\theta,\varphi,t) = \tilde{x}(r) + x'(r,\theta,\varphi,t), \quad \frac{|x'|}{|x|} \ll 1, \quad \forall (r,\theta,\varphi,t), \tag{2}$$

where (r,θ,φ) are the spherical coordinates and t is the time.

5.1 Reference state from MESA

We use MESA to produce a 1D reference state with default settings of a non-rotating, $3M_\odot$ zero-age main sequence star of metallicity $Z = 0.02$ without convective overshooting. The total radius of the star is $2.04R_\odot$ and its luminosity is $85L_\odot$. The profiles of density, temperature, and gravity are approximated using polynomial fits of degree fourteen (Fig. 4). The Brunt–Väisälä frequency N obtained from MESA is used to distinguish between the convective zone ($N^2 < 0$) and the radiative zone ($N^2 > 0$). The interface between the two is marked with a red vertical line in Fig. 5a.

5.2 MagIC code

MagIC is a 3D anelastic MHD code to simulate fluids in a rotating sphere or in spherical shells. It is a pseudo-spectral code and uses Chebyshev spectral methods or finite differences in the radial direction and spherical harmonic decomposition in the azimuthal and latitudinal directions. MagIC relies on a hybrid parallelisation scheme using both MPI and

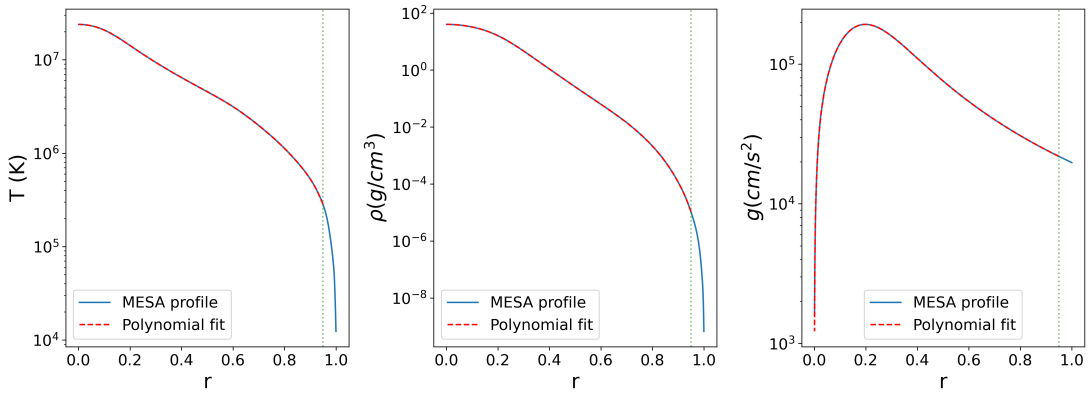

Figure 4: The reference state profiles form MESA as a function of the normalised radius r and their polynomial fit from the center $r = 0$ to the cutoff radius $r = 0.95$ (the green dashed line). Left panel: background temperature profile. Middle panel: background density profile. Right panel: gravity profile.

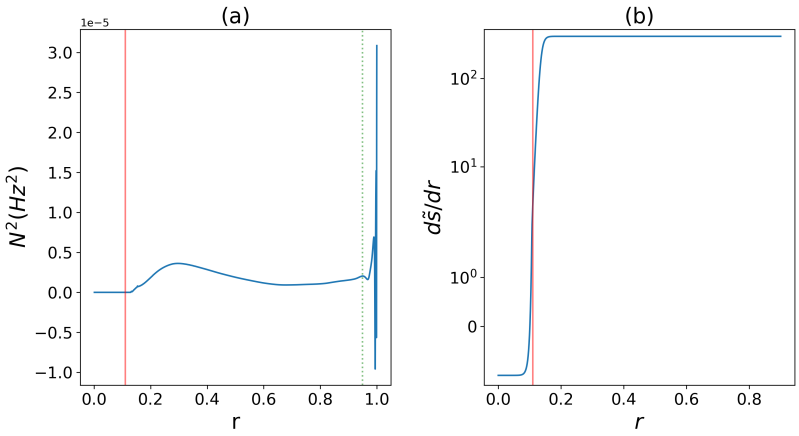

Figure 5: The profiles of the Brunt–Väisälä frequency squared (a) and the imposed dimensionless background entropy gradient (b) as a function of the normalised radius r (the red line represent the convective/radiative interface).

OpenMP. We use MagIC to solve the conservation of momentum equation

$$\left(\frac{\partial \vec{u}}{\partial t}+\vec{u}\cdot\vec{\nabla}\vec{u}\right)=-\vec{\nabla}\left(\frac{p'}{\tilde{\rho}}\right)-\frac{2}{E}\vec{e}_z\times\vec{u}+\frac{Ra}{Pr}\tilde{g}s'\vec{e}_r+\frac{1}{\tilde{\rho}}\vec{\nabla}\cdot\mathrm{S}, \tag{3}$$

the continuity equation

$$\vec{\nabla}\cdot\tilde{\rho}\vec{u}=0, \tag{4}$$

and the energy equation

$$\tilde{\rho}\tilde{T}\left(\frac{\partial s'}{\partial t}+\vec{u}\cdot\vec{\nabla}s'\right)=\frac{1}{Pr}\vec{\nabla}\cdot\left(\kappa(r)\tilde{\rho}\tilde{T}\vec{\nabla}s'\right)+\frac{\mathrm{Pr}\,Di}{Ra}\Phi_\nu, \tag{5}$$

in a full sphere. Here, $\vec{u}$ is the velocity field, p the modified pressure that includes centrifugal forces, ρ the density, T the temperature and s the entropy. Using the radius of the sphere as the length scale and the viscous diffusion time as time scale, we get the following non-dimensional numbers. $E=\frac{\nu}{\Omega R_o^2}$ denotes the Ekman number, $Ra=\frac{\alpha_o g_o T_o R_o^3 \Delta s}{c_p \kappa_o \nu_o}$ the thermal Rayleigh number and $\mathrm{Pr}=\frac{\nu_o}{\kappa_o}$ the Prandtl number. Here, c_p, ν and κ denote the specific heat at constant pressure, kinematic viscosity and thermal diffusivity, respectively and the subscript o denotes the outer boundary or surface of the sphere. The 1D reference profiles from MESA complete the equations by providing a gravity profile and an equation of state.

To control the location and the degree of stratification of the stably stratified envelope, we use a functional form of the background entropy gradient $\mathrm{d}\tilde{s}/\mathrm{d}r$ prescribed in MagIC. Regions with a negative gradient are super-adiabatic while the fluid layers with positive gradient are stably stratified. Here, we assume a constant degree of stratification $\mathrm{d}\tilde{s}/\mathrm{d}r=\Gamma_s=300$ between $\mathcal{R}_i=0.11$ and the outer boundary ($\mathcal{R}_o$) and a constant dimensionless negative gradient $\mathrm{d}\tilde{s}/\mathrm{d}r=-1$ in the convective core. These regions are then smoothly connected with

$$\frac{\mathrm{d}\tilde{s}}{\mathrm{d}r}=\frac{1+\Gamma_s}{4}\left[1+f_{\mathcal{R}_i}(r)\right]\left[1-f_{\mathcal{R}_o}(r)\right], \tag{6}$$

where

$$f_a(r)=\tanh\left[\zeta_s(r-a)\right], \quad \mathcal{R}_o=\mathcal{R}_i+\mathcal{H}_s. \tag{7}$$

We set the stiffness of the transition ζ_s to 75 and the thickness of the stably stratified layer $\mathcal{H}_s$ to a large number to cover all the envelope (Fig. 5b).

In our simulation, we assume the outer boundary to be stress-free and have a fixed entropy flux. We initialise the entropy and velocity fields with random noise. Additionally, we assume that the kinematic viscosity and the thermal diffusivity are constants. Finally, we set the dimensionless numbers to $\mathrm{Ra}=10^{10}$, $\mathrm{Ek}=10^{-6}$ and $\mathrm{Pr}=1$, and the cutoff radius to 50% of the stellar radius for numerical convenience.

5.3 Preliminary results

5.3.1 Onset of turbulent convection and wave generation

In Fig. 6, we see 2D snapshots of the radial velocity in the equatorial plane and a meridional and an equatorial slice of the azimuthal velocity. We take the snapshots at an early moment of the formation of the turbulent convection from the evolution of the random noise that we begin the simulation with. The effective Ekman number in the convection zone is $Ek/r_c^2=4\times10^{-6}$, which is low enough to have a large rotational effect. This is seen in the columnar nature of convection. Shortly after the onset of convection, we can see wave-like flows being generated in the radiative zone which till now was in solid body rotation. An equatorial slice of zonal flow also shows the radiative zone starting to gain some angular momentum.

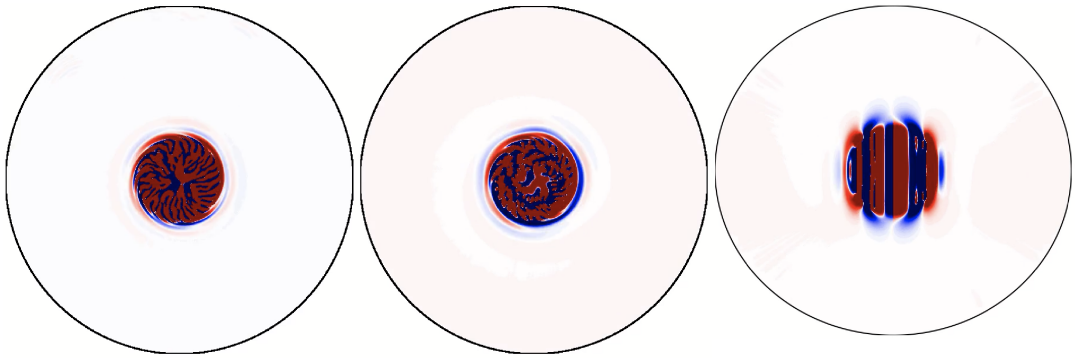

Figure 6: Formation of the turbulent convection from the random noise and generation of the GIWs at $t_{\rm visc} = 1.25 \times 10^{-3}$. Left panel: Equatorial slice of the radial velocity. Middle panel: Equatorial slice of the azimuthal velocity. Right panel: Meridional slice of the azimuthal velocity.

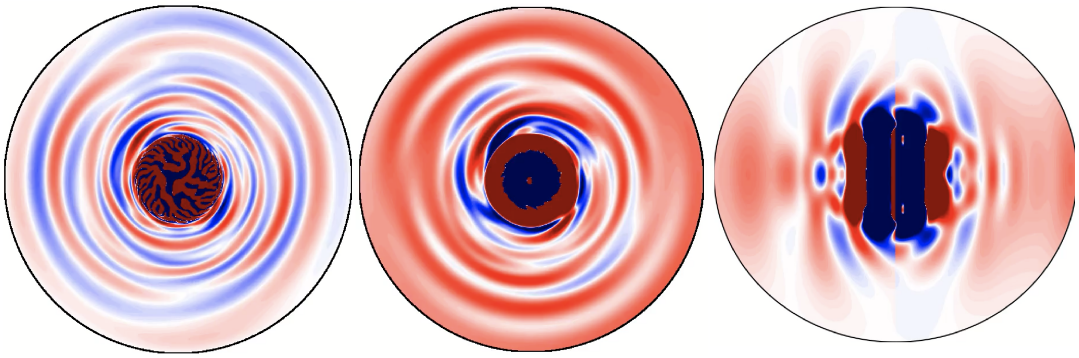

Figure 7: Same as Fig. 6 but at $t_{visc} = 1.6 \times 10^{-3}$.

5.3.2 GIWs propagation

Fig. 7 shows the same views as Fig. 6 but in a statistically stationary state of the simulation. We can see that the initial weak flows in the radiative zone are now stronger and well developed and propagation of GIWs can be observed when playing movies of these views. We can see in the snapshot of the meridional slice of the azimuthal velocity (right panel) that the waves seem to form global modes. Furthermore, the waves are trapped near the equator due to the small vertical extent of the convection zone which produces the flows impinging on the interface leading to GIW formation. The flows in the radiative zone develop a columnar structure as well due to the effect of rotation.

In Fig. 8, we see some 3D snapshots of entropy and radial velocity at a viscous diffusion time 1.93×10^{-3} in a statistically stationary state. We can see in the convective core what we believe to be plumes (in the right panel) that penetrate the radiative envelope and perturb it leading to the formation of the GIWs in the envelope. The wave-like flows seen in our simulations look very similar to those shown in Rogers et al. (2013) and Edelmann et al. (2019).

5.3.3 Angular momentum transport

We recall that specific angular momentum is defined by

$$\mathcal{L}(r, \varphi, t) = (r \sin\theta)^2 \Omega = r \sin\theta \left(\bar{v}_\varphi + r \sin\theta \Omega_0\right), \tag{8}$$

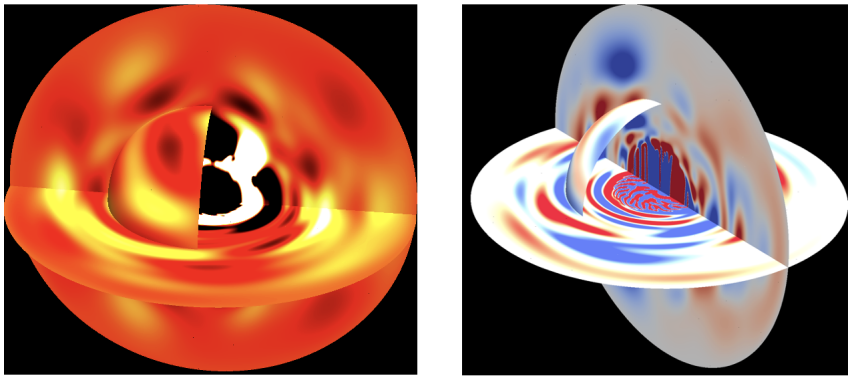

Figure 8: 3D visualisation of the entropy (left panel) and the radial velocity (right panel) at $t_{\rm visc} = 1.93 \times 10^{-3}$ (viscous time scale).

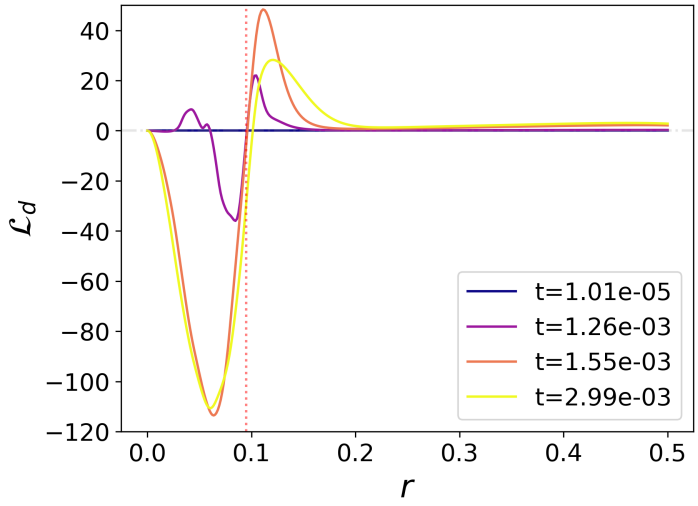

Figure 9: Specific angular momentum change as a function of the radius at different time steps (the red dashed line is the radiative/convective interface).

where Ω_0 is the initial angular velocity and $\bar{v}_\varphi$ is the azimuthal velocity averaged over φ in the rotating frame. In order to visualize how the angular momentum has evolved compared to that of the initially imposed uniform rotation, we examine the quantity

$$\mathcal{L}_d(r,t) = \int_0^\pi (\mathcal{L} - \mathcal{L}_0) \sin\theta \mathrm{d}\theta, \tag{9}$$

at different time steps. Here, $\mathcal{L}_0 = (r\sin\theta)^2\Omega_0$ is the initial specific angular momentum. This quantity expresses the change in angular momentum with respect to uniform rotation, integrated on horizontal surfaces. Fig. 9 shows a plot of $\mathcal{L}_d$ as a function of radius at different time steps. We can see that the angular momentum is extracted from the internal part of the convective core then, transported to the internal radiative zone and finally, deposited near the outer boundary.

6 Conclusion and perspective

We performed 3D hydrodynamic simulations of an intermediate-mass star using the MagIC code while using 1D reference profiles of interior properties from the stellar evolution code MESA. We used a profile of background entropy gradient to define the convective and radiative zones. We found that convective forcing at the interface gave rise to gravito-inertial waves (GIWs) in the radiative zone. Though it is yet to be quantitatively studied, GIWs seem to deposit angular momentum near the surface of the simulated star. However, a lot of open questions remain. First and foremost, we need to quantify the spectrum of GIWs obtained in the simulation and compare them with that obtained using eigenvalue computations from `GYRE` (Townsend and Teitler, 2013; Townsend et al., 2018). Secondly, we need to quantify the angular momentum transport by GIWs and their dissipation. Thirdly, we need to perform a parameter study to see how sensitive the GIW properties are to our chosen non-dimensional numbers. Yet another step would be to add realistic profiles of transport properties and heat sources. Lastly, we need to study the effect of changing the simulation domain to more than 50% of the star. A planned step is to try and simulate 70% and thereafter attempt to simulate 90% of the star. This project thus has a rich prospect and opens up various avenues of research into modeling of intermediate-mass stars in general and study of angular momentum transport by GIWs in particular.

References

C. Aerts, S. Mathis, and T. M. Rogers. Angular momentum transport in stellar interiors. *Annual Review of Astronomy and Astrophysics*, 57(1):35–78, 2019. doi: 10.1146/annurev-astro-091918-104359. URL `https://doi.org/10.1146/annurev-astro-091918-104359`.

L. Alvan, A. S. Brun, and S. Mathis. Theoretical seismology in 3d: nonlinear simulations of internal gravity waves in solar-like stars. *A&A*, 565:A42, 2014. doi: 10.1051/0004-6361/201323253. URL `https://doi.org/10.1051/0004-6361/201323253`.

L. Alvan, A. Strugarek, A. S. Brun, S. Mathis, and R. A. Garcia. Characterizing the propagation of gravity waves in 3d nonlinear simulations of solar-like stars. *A&A*, 581:A112, 2015. doi: 10.1051/0004-6361/201526250. URL `https://doi.org/10.1051/0004-6361/201526250`.

Q. André. *Ondes gravito-inertielles dans les étoiles et les planètes géantes : propagation, dissipation et échanges de moment cinétique*. PhD thesis, Université de Paris, 2019. URL `http://www.theses.fr/2019UNIP7073`.

K. C. Augustson, A. S. Brun, and J. Toomre. THE MAGNETIC FURNACE: INTENSE CORE DYNAMOS IN b STARS. *The Astrophysical Journal*, 829(2):92, sep 2016. doi: 10.3847/0004-637x/829/2/92. URL `https://doi.org/10.3847/0004-637x/829/2/92`.

S. I. Braginsky and P. H. Roberts. Equations governing convection in earth's core and the geodynamo. *Geophysical & Astrophysical Fluid Dynamics*, 79(1-4):1–97, 1995. doi: 10.1080/03091929508228992. URL `https://doi.org/10.1080/03091929508228992`.

A. S. Brun, M. S. Miesch, and J. Toomre. Global-scale turbulent convection and magnetic dynamo action in the solar envelope. *The Astrophysical Journal*, 614(2):1073–1098, oct 2004. doi: 10.1086/423835. URL `https://doi.org/10.1086/423835`.

T. Clune, J. Elliott, M. Miesch, J. Toomre, and G. Glatzmaier. Computational aspects of a code to study rotating turbulent convection in spherical shells. *Parallel Computing*, 25(4):361–380, 1999. ISSN 0167-8191. doi: https://doi.org/10.1016/S0167-8191(99)00009-5. URL https://www.sciencedirect.com/science/article/pii/S0167819199000095.

P. V. F. Edelmann, R. P. Ratnasingam, M. G. Pedersen, D. M. Bowman, V. Prat, and T. M. Rogers. Three-dimensional simulations of massive stars. i. wave generation and propagation. *The Astrophysical Journal*, 876(1):4, apr 2019. doi: 10.3847/1538-4357/ab12df. URL https://doi.org/10.3847/1538-4357/ab12df.

T. Gastine and J. Wicht. Effects of compressibility on driving zonal flow in gas giants. *Icarus*, 219(1):428–442, 2012. ISSN 0019-1035. doi: https://doi.org/10.1016/j.icarus.2012.03.018. URL https://www.sciencedirect.com/science/article/pii/S001910351200111X.

S. R. Lantz and Y. Fan. Anelastic magnetohydrodynamic equations for modeling solar and stellar convection zones. *The Astrophysical Journal Supplement Series*, 121(1):247–264, mar 1999. doi: 10.1086/313187. URL https://doi.org/10.1086/313187.

B. Paxton, L. Bildsten, A. Dotter, F. Herwig, P. Lesaffre, and F. Timmes. Modules for Experiments in Stellar Astrophysics (MESA). *The Astrophysical Journal Supplement Series*, 192:3, jan 2011. doi: 10.1088/0067-0049/192/1/3.

B. Paxton, M. Cantiello, P. Arras, L. Bildsten, E. F. Brown, A. Dotter, C. Mankovich, M. H. Montgomery, D. Stello, F. X. Timmes, and R. Townsend. Modules for Experiments in Stellar Astrophysics (MESA): Planets, Oscillations, Rotation, and Massive Stars. *Astrophysical Journal Supplement Series*, 208:4, sep 2013. doi: 10.1088/0067-0049/208/1/4.

B. Paxton, P. Marchant, J. Schwab, E. B. Bauer, L. Bildsten, M. Cantiello, L. Dessart, R. Farmer, H. Hu, N. Langer, R. H. D. Townsend, D. M. Townsley, and F. X. Timmes. Modules for Experiments in Stellar Astrophysics (MESA): Binaries, Pulsations, and Explosions. *Astrophysical Journal Supplement Series*, 220:15, sep 2015. doi: 10.1088/0067-0049/220/1/15.

B. Paxton, J. Schwab, E. B. Bauer, L. Bildsten, S. Blinnikov, P. Duffell, R. Farmer, J. A. Goldberg, P. Marchant, E. Sorokina, A. Thoul, R. H. D. Townsend, and F. X. Timmes. Modules for Experiments in Stellar Astrophysics (MESA): Convective Boundaries, Element Diffusion, and Massive Star Explosions. *The Astrophysical Journal Supplement Series*, 234:34, feb 2018. doi: 10.3847/1538-4365/aaa5a8.

B. Paxton, R. Smolec, J. Schwab, A. Gautschy, L. Bildsten, M. Cantiello, A. Dotter, R. Farmer, J. A. Goldberg, A. S. Jermyn, S. M. Kanbur, P. Marchant, A. Thoul, R. H. D. Townsend, W. M. Wolf, M. Zhang, and F. X. Timmes. Modules for Experiments in Stellar Astrophysics (MESA): Pulsating Variable Stars, Rotation, Convective Boundaries, and Energy Conservation. *The Astrophysical Journal Supplement Series*, 243(1):10, Jul 2019. doi: 10.3847/1538-4365/ab2241.

T. M. Rogers. ON THE DIFFERENTIAL ROTATION OF MASSIVE MAIN-SEQUENCE STARS. *The Astrophysical Journal*, 815(2):L30, dec 2015. doi: 10.1088/2041-8205/815/2/l30. URL https://doi.org/10.1088/2041-8205/815/2/l30.

T. M. Rogers, D. N. C. Lin, J. N. McElwaine, and H. H. B. Lau. INTERNAL GRAVITY WAVES IN MASSIVE STARS: ANGULAR MOMENTUM TRANSPORT. *The Astrophysical Journal*, 772(1):21, jul 2013. doi: 10.1088/0004-637x/772/1/21. URL https://doi.org/10.1088/0004-637x/772/1/21.

R. H. D. Townsend and S. A. Teitler. GYRE: an open-source stellar oscillation code based on a new Magnus Multiple Shooting scheme. *MNRAS*, 435(4):3406–3418, Nov. 2013. doi: 10.1093/mnras/stt1533.

R. H. D. Townsend, J. Goldstein, and E. G. Zweibel. Angular momentum transport by heat-driven g-modes in slowly pulsating B stars. *MNRAS*, 475(1):879–893, Mar. 2018. doi: 10.1093/mnras/stx3142.

W. Unno, Y. Osaki, H. Ando, H. Saio, and H. Shibahashi. *Nonradial oscillations of stars*. 1989.

J. Wicht. Inner-core conductivity in numerical dynamo simulations. *Physics of the Earth and Planetary Interiors*, 132(4):281–302, 2002. ISSN 0031-9201. doi: https://doi.org/10.1016/S0031-9201(02)00078-X. URL https://www.sciencedirect.com/science/article/pii/S003192010200078X.